V. Muscarello, G. Quaranta, P. Masarati
The Role of Rotor Coning in Helicopter Proneness to Collective Bounce
Aerospace Science and Technology, Vol. 36, 2014, p. 103-113
doi:10.1016/j.ast.2014.04.006

The Role of Rotor Coning in Helicopter Proneness to Collective Bounce

Vincenzo Muscarello, Giuseppe Quaranta, Pierangelo Masarati

Dipartimento di Scienze e Tecnologie Aerospaziali, Politecnico di Milano, Italy

Abstract

Collective bounce is a rotorcraft-pilot coupling phenomenon caused by vertical vibrations in the aircraft cockpit that are transmitted to the collective lever through the torso, the left arm and the hand of the pilot, and fed back to the rotor through the collective pitch control. This paper shows that collective bounce is rooted in the coupling of the pilot biodynamics with the rotor coning mode. The damping of the coning mode, usually large, introduces significant phase delay in the response to collective pitch. When coupled in feedback with the pilot biodynamics, such delay may lead to marginal stability conditions or even to instability. The basic mechanism of this coupling is shown using simple analytical models, and confirmed using detailed helicopter models. The influence of several design parameters is investigated, and possible means of prevention are briefly discussed.

Keywords: Rotorcraft-pilot couplings, biodynamic feedthrough, collective bounce

1. Introduction

ROTORCRAFT, like most vehicles, can be subjected to adverse interaction with the pilot. In fact the pilot, as a consequence of misleading or incorrectly interpreted cues, can move the control inceptors in a manner that produces inadvertent or unintentional commands. These commands, in turn, can produce a behavior of the vehicle that causes further misleading cues, and induce additional adverse input, potentially resulting in unstable events, called Aircraft-Pilot Couplings (APC) in general, and Rotorcraft-Pilot Couplings (RPC) when specifically referred to rotary wing aircraft.

The most renowned and investigated occurrences of A/RPCs are known as Pilot Induced Oscillations (PIO), a name that refers to an oscillatory behavior of the vehicle resulting from commands intentionally introduced by the pilot in response to misinterpreted or contradictory cues. Well-known A/RPCs of different nature are known as Pilot Assisted Oscillations, or Pilot Augmented Oscillations (PAO), where the oscillatory behavior results from involuntary commands produced by the pilot, often caused by vibrations of the vehicle. Although both names have been criticized because they put all the blame on the pilots (McRuer [1]), they highlight an essential feature of the phenomenon, namely its oscillatory nature (Mitchell and Klyde [2]).

PIOs are characterized by voluntary pilot intervention; the pilot "fights" against the aircraft when its behavior contradicts the mental model of the vehicle the pilot formed in his mind. As a consequence, PIOs

usually occur in a band of frequencies pilots can normally control. Based on a literature survey, during activity performed under the umbrella of GARTEUR[1] Helicopter Action Group HC AG-16, the upper limit of such band was conventionally placed at 1 Hz [3]. PAOs are characterized by unintentional pilot intervention; the pilot inadvertently feeds undesired controls to the aircraft as a result of the vibrations induced by the interface with the cockpit. The frequency band that characterizes the phenomenon is above that of PIO, where the pilot is no longer capable of intentionally introducing commands, and below an upper limit that was conventionally set at about 8 Hz in [3]. In fact, from that frequency on, the biomechanics of the human body filters out any motion caused by the cockpit.

While PIO and PAO have been investigated in detail in relation to fixed wing aircraft [4, 5, 6, 7], and PIO is receiving considerable attention in relation with rotary wing aircraft [8, 9, 10], PAO received less attention. This contrasts with the fact that frequencies characteristic of many aspects of rotorcraft aeromechanics — flight mechanics, rotor aeromechanics, airframe, drive train, and engine dynamics — also lie in this range. Several occurrences of PAO in rotorcraft are listed in [11, 9]. Noteworthy cases related to US Navy vehicles have been discussed in [12]. A possible case of PAO occurred during the development of the AH-56 Cheyenne compound helicopter is discussed in Section "Lesson learned No. 9 (again)" of [13]. PAO events occurred during the development of the V-22 tiltrotor are discussed in [14].

A PAO phenomenon specific of helicopters is the so-called "collective bounce", an RPC caused by vertical vibrations of the cockpit. As a consequence of the most common cockpit and control inceptors layout, the vibrations induce a collective control input as a result of the biodynamics of the pilot's left arm. This, in turn, further excites the vertical vibration by directly inducing a change in rotor thrust along the vertical axis.

Even recently, the National Transportation Safety Board (NTSB) reported accidents occurred after encountering collective bounce (reports[2] SEA08LA043 and ANC08LA083, respectively related to accidents occurred in December 2007 and June 2008). In both cases, a UH-1B was involved, and the probable cause was related to failure of the pilot in controlling the collective bounce. In one case this was accompanied by insufficient collective control friction; in the other by poor maintenance, resulting in loose and worn control system and rotor bearings. The NTSB reports indicate that

> According to the Operator's Manual for the UH-1B helicopter, "Collective bounce is a pilot induced vertical oscillation that may be encountered in any flight condition by a rapid buildup of vertical bounce at approximately three cycles per second. The severity of this oscillation is such that effective control of the aircraft may become difficult to maintain."

A change in collective pitch essentially results in a very quick change in thrust, since the dynamics of the

[1] `http://www.garteur.org/`, last accessed July 2013.

[2] `http://www.ntsb.gov/aviationquery/`, last accessed July 2013

aerodynamics may be regarded as fast in relation with the frequency that characterizes the phenomenon, usually below 1/rev (once per revolution). A thrust change, in turn, produces a vertical acceleration. If the pilot's biomechanics, at least in part, transforms this acceleration into a rotation of the collective inceptor, inducing a further change in rotor blade collective pitch, a feedback loop appears, that may lead to collective bounce.

One may be tempted to explain the phenomenon directly through such mechanism. However, this work shows that a key role in emphasizing collective bounce is played by the collective flap, or coning, rotor mode. Helicopter rotor blades are allowed to flap, namely move out of the rotor disk plane by either rotating about a hinge orthogonal to both the blade and the rotor axis and located close to the blade root (articulated rotors), or by bending a flexural element that connects the blade root to the hub (hingeless rotors). As a consequence of such displacement, the blade is in equilibrium about the flap hinge under the aerodynamic and centrifugal loads, relieving the blade itself from carrying lift to the hub in form of bending moment. Perturbations of such equilibrium result in flapping dynamics characterized by a natural frequency close to (and usually slightly higher than) the rotor angular velocity, and by significant damping provided by the aerodynamics, since the local angle of attack of the blades is modified by the flapping velocity. When all blades flap simultaneously, the rotor coning mode occurs. This mode is known to be highly damped (between 35% and 50%, with notable exceptions), which implies limited amplification, if any, even at resonance. What makes the coning mode dominate the proneness to collective bounce is actually the phase delay introduced in rotor thrust by this mode, something not acknowledged so far, to the authors' knowledge.

A simple analytical model of the problem is presented in Section 2. The model points out the dependence of collective bounce on the interaction between the biomechanics of the pilot and the rotor coning mode. Specifically, the role of the phase lag introduced by rotor coning in the loop transfer function between the blade collective pitch and the involuntary pitch control induced by the vertical acceleration of the helicopter as a consequence of biodynamic feedthrough is highlighted. How effectively the minimal model captures the essence of the problem, compared to more sophisticated aeromechanics models, is discussed in Section 3, along with an exhaustive discussion of the sensitivity of the phenomenon to the most important parameters of the problem. Possible means of prevention are briefly discussed in Section 4.

2. Analytical Model

In hover, rotors respond to changes in blade collective pitch with collective flap motion. This motion is called the rotor blade coning motion, and is described by the collective flap angle β_0. The basics of rotor blade flapping coupled with helicopter vertical motion in hover are briefly reviewed in this section. The objective is to formulate the equations of motion that characterize the helicopter dynamics that may be relevant for the involuntary interaction with the pilot during collective bounce.

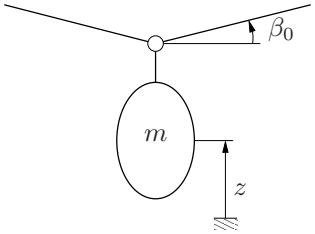

Figure 1: Sketch of the minimal analytical model of the helicopter associated with pure heave (z) and collective coning (β_0) motion.

A simplified model is developed, sketched in Fig. 1, which consists of the vertical motion of the entire helicopter and the rotor coning motion. The model is drastically simplified, since it neglects the details of the rotor hub geometry and kinematics (for example the pitch-flap coupling, which provides an aerodynamic contribution to the equivalent stiffness of blade flapping), the drive train dynamics (which in principle could interact with collective flap and pitch motion), and many details of basic rotor aerodynamics like inflow, twist, tip loss etc., that may be significant in performance analysis but are considered inessential for the desired perturbative model, or require not readily available or easily accessible information. Specifically, inflow dynamics has been neglected from the beginning to avoid excessive complication of the analytical model, and the validity of the assumption has been verified later using numerical models obtained from comprehensive rotorcraft analysis.

2.1. Basic Blade Flapping Dynamics

A rotorcraft in hover is considered. For simplicity, the model consists of rigid, articulated blades whose motion relative to the hub is restricted to flapping, with null flap hinge offset; the effect of the offset on blade dynamics is recovered using an equivalent flap spring of stiffness $k_\beta = I_\beta(\nu_\beta^2 - 1)$, such that the nondimensional natural flap frequency of the isolated rotor in vacuo is ν_β. Inflow, tip losses, root cut-out and pre-twist are neglected for simplicity, since in this context they would only introduce a correction of the resulting coefficients without altering the key relationships between the parameters that characterize the motion. The relative participation of aerodynamic and inertial forces is described by the Lock number,

$$\gamma = \frac{\rho a c R^4}{I_\beta}, \tag{1}$$

where ρ is the air density (international standard atmosphere (ISA) was considered in this work), a is the lift curve slope, c is the chord, R is the rotor radius, and I_β is the flap inertia moment. In a general discussion of rotor aeromechanics, the perturbative flap angle β, pitch angle θ and vertical motion z would be expressed as functions of their azimuthal harmonic decomposition. Since this work focuses on perturbation of hover along the vertical axis, only the collective (i.e. uniform with respect to azimuth) term of the kinematic

parameters is considered, yielding a set of linear time invariant equations,

$$m\ddot{z} + n_b\frac{\gamma}{4}\Omega\frac{I_\beta}{R^2}\dot{z} + n_b S_\beta\ddot{\beta} + n_b\frac{\gamma}{6}\Omega\frac{I_\beta}{R}\dot{\beta} = n_b\frac{\gamma}{6}\Omega^2\frac{I_\beta}{R}\theta \tag{2a}$$

$$n_b I_\beta\ddot{\beta} + n_b\frac{\gamma}{8}\Omega I_\beta\dot{\beta} + n_b I_\beta\nu_\beta^2\Omega^2\beta + n_b S_\beta\ddot{z} + n_b\frac{\gamma}{6}\Omega\frac{I_\beta}{R}\dot{z} = n_b\frac{\gamma}{8}\Omega^2 I_\beta\theta; \tag{2b}$$

the symbols are defined in Table 1. Equation (2a) describes the vertical displacement of the helicopter, and Eq. (2b) describes the rotor coning. Coupling occurs thanks to inertia forces, by way of the static moment S_β of the blades, and to aerodynamics, by way of the change in angle of attack related to the vertical velocity of the aircraft, $\dot{z}$, and to the blade flapping rate, $\dot{\beta}$.

In the following, the simplified helicopter model is essentially seen as a Single Input/Single Output (SISO) system in the Laplace domain in the form

$$z(s) = H_{z\theta}\theta(s). \tag{3}$$

A minimal, definitely unrealistic model is obtained by eliminating the rotor coning dynamics, i.e. by imposing $\beta = 0$.

2.2. Discussion on Rotor Coning

The first part of this work is based on rather simplified models. The analysis is rooted in data that are specific of typical helicopter designs. To support the discussion, six helicopters are considered: one with teeter main rotor, the Bell AB204; three with articulated main rotor, the Sud Aviation (now Airbus helicopters) SA330 Puma, the Sikorsky CH-53 Sea Stallion and UH-60 Black Hawk; two with hingeless main rotor, the Bölkow (now Airbus Helicopters) BO105 and Westland (now AgustaWestland) Lynx. They significantly differ in size, rotor design and properties, as shown in Table 1. Data have been collected from heterogeneous sources and, in some cases, estimated using simplified methods; as a consequence, they should only be considered indicative of helicopters of the corresponding classes and main rotor designs.

Data for the AB204 have been collected from various sources; specifically, blade structural properties were obtained from [15], a work that presents a modal survey of an isolated AB204 main rotor blade, and the corresponding $\nu_\beta = 1.2$ was estimated using a finite element analysis assuming uniform blade mass and bending stiffness distribution; $\gamma = 6.8$ has been estimated accordingly. Data for the BO105, SA330, and Lynx come in part from [16] and other sources. Data for the CH-53 come from [17], whereas data for the UH-60 have been obtained from [18].

Temporarily restricting the motion to flapping ($z = 0$), the coning equation, Eq. (2b), is characterized by a frequency that in vacuo (i.e. for $\gamma = 0$) may vary from between slightly above 1/rev and 1.03/rev for an articulated rotor, up to 1.1/rev for a hingeless rotor, to 1.2/rev and more for a teeter (i.e. semi-rigid)

Table 1: Simplified models data.

		AB204	SA330[a]	CH-53	UH-60	BO105	Lynx
Rotor type		teeter	articulated	articulated	articulated	hingeless	hingeless
Total mass	m (kg)	4310.0	7345.0	15227.0	7537.0	2055.0	4313.7
Number of blades	n_b	2	4	6	4	4	4
Rotor radius	R (m)	7.32	7.49	11.01	8.18	4.9	6.4
Rotation speed	Ω (Hz)	4.9	4.5	3.07	4.3	7.07	5.67
Lock number	γ	6.8[b]	8.7	12.4[b]	8.2	4.31	7.12
Blade mass	m_b (kg)	88.0	91.64	135.84[c]	116.5	50.61	49.67[c]
Flap static moment	S_β (kg·m)	322.1[d]	276.48	819.0	385.7	80.17	158.94[d]
Flap inertia moment	I_β (kg·m^2)	1571.8[e]	1339.19	5489.0	2052.1	249.85	678.14
Flap frequency ratio	ν_β	1.2[f]	1.029	1.048	1.035	1.076	1.092
Coning mode damping	ξ_β	0.35	0.53	0.74	0.49	0.25	0.41
Heave time constant[g]	T (s)	1.40	1.25	0.94	1.04	1.03	1.03

[a]Heavy version. [b]Computed from Eq. (1). [c]Estimated: $m_b = 3I_\beta/R^2$. [d]Estimated: $S_\beta = m_b R/2$. [e]Estimated: $I_\beta = m_b R^2/3$. [f]Computed using a finite element model of a blade with uniform mass and bending stiffness distribution. [g]Computed from Eq. (10).

design, as shown in Table 1 (Blackwell and Millott in [19] report 1.5/rev for the Sikorsky X2 compound, coaxial slowed rotor technology demonstrator, not considered in this work).

Rotor coning is a highly damped mode. The damping factor is

$$\xi = \frac{\gamma}{16\nu_\beta} \cong \frac{\gamma}{16}. \tag{4}$$

For typical main rotor designs $\gamma \approx 8$, resulting in about 50% damping of the coning mode; according to Table 1, coning mode damping ranges between 35% and 75%.

The problem of Eq. (2) is characterized by a pole in the origin, corresponding to a rigid displacement of the system, a real pole corresponding to a(n almost) rigid translation of the system with non-null velocity, and two poles associated with the coning motion. The latter two poles are complex conjugated for typical values of rotor parameters (for example, for all the cases considered in Table 1). The coning motion is coupled to the vertical displacement by inertia and aerodynamic forces. The natural frequency of the coning mode is very close to that of an isolated rotor, $\nu_\beta\Omega$. In air, the imaginary part of the eigenvalues, $\nu_\beta\Omega\sqrt{1-\xi^2}$, can be significantly less, down to 70% of $\nu_\beta\Omega$, because of the damping. The reduced frequency κ associated

with the coning mode at radial station $r = \zeta R$ is

$$\kappa = \frac{\omega c}{2v(r)} = \frac{\nu_\beta \Omega c}{2\zeta R \Omega} = \frac{\nu_\beta}{2\zeta}\frac{c}{R}. \tag{5}$$

For $\zeta = 0.8$, a station about which most of the aerodynamic load is produced, κ can be up to about 0.05. Such value is small enough for a steady aerodynamic model to be acceptable as a first approximation, although not accurate enough for a quantitative analysis. This implies that aerodynamic forces may not adapt instantaneously pitch changes; response to collective pitch may suffer from additional delay of aerodynamic nature. In fact, Theodorsen's unsteady aerodynamics theory predicts a phase delay of about 8 deg at a reduced frequency of 0.05, i.e. a time delay of about $0.15/(\nu_\beta\Omega)$ s, between 3 ms and 7 ms for the helicopters considered in Table 1.

The coning mode is intrinsic in rotor aeromechanics; it could be eliminated or at least significantly modified only by a radical redesign of rotor blade dynamics (e.g. designing very stiff, propeller-like rotors), which is likely to be incompatible with other requirements. However, considering the minimal amplification associated with such a highly damped mode, one may question whether it is essential in a simplified collective bounce analysis. This work shows how the presence of that mode can have a very important role in proneness to collective bounce.

2.3. Involuntary Collective Control Loop Closure

The collective control is actuated as a consequence of two logically distinct contributions originating from the pilot, as shown in Fig. 2. The first contribution is the result of the intentional action performed by the pilot to control the vehicle. Based on the perceived cues, the pilot operates the collective control to perform the desired task, which may vary from controlling the altitude of the helicopter while hovering in close proximity to the terrain (often a high precision task) to controlling the climb or descent rate (usually a low precision task that can be obtained by considering very far visual cues). This contribution is called Active Pilot (AP) in the following.

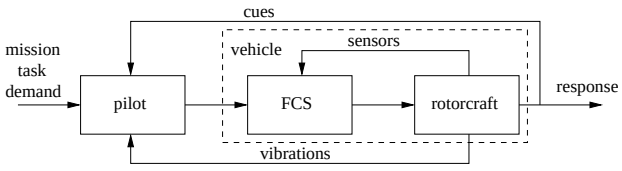

Figure 2: Block diagram of pilot-vehicle interaction.

The second contribution originates from vibrations produced by the aircraft and filtered by the pilot's biodynamics. These vibrations come from the interface between the pilot and the cockpit. As a consequence of such excitation, the pilot's arms vibrate while holding the control inceptors, resulting in the introduction of involuntary controls. This contribution is called Passive Pilot (PP) in the following.

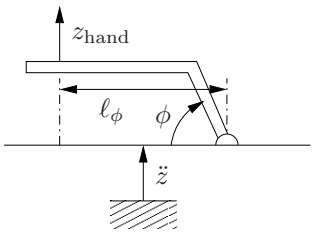

Figure 3: Sketch of collective control inceptor.

2.4. Collective Control Inceptor

The collective control inceptor, sketched in Fig. 3, usually provides minimal force feedback; thus no force other than that exerted by the pilot contrasts the motion of the lever when the pilot commands it. However, to improve the quality of its positioning, and in the end the "touch and feel" of the pilot, some force threshold needs to be overcome in order to move the lever from rest. In helicopters controlled by direct mechanical transmission of the command, this effect is produced by some artificial friction that resists the motion of the lever. The minimum amount of friction is usually prescribed by the manufacturer, and the actual amount can be adjusted to best suit the pilot's needs.

In the present analysis, friction is not directly considered, since it is hard to deal with in linear frequency domain models, but rather implicitly accounted for in the transfer function identified from experimental measures; the stick-slip effect associated with transition from pure adhesion to sliding and vice versa is omitted. This simplification is considered conservative.

The motion of the collective control inceptor prescribes the collective pitch angle of the rotor blades. In augmented control helicopters, the motion of the control is the collective pitch demand to actuators, either directly or through a Flight Control System (FCS). In usual arrangements, the full range $\Delta\phi$ of the control lever rotation, ϕ, is about 40 to 45 degrees for a lever length ℓ_ϕ of about 0.28 to 0.35 m from the hinge to the hand grip. An estimate of the ratio between the displacement of the hand and the non-dimensional rotation η of the lever is thus

$$\eta = \frac{\phi}{\Delta\phi} = \frac{1}{\ell_\phi \Delta\phi} \cdot z_{\text{hand}}, \tag{6}$$

where z_{hand} is the displacement of the hand. The collective pitch range of a helicopter, $\Delta\theta$, is of the order of 20 degrees, a reasonable value for G_c, the ratio between the non-dimensional rotation of the control and the blade pitch. In conclusion, the ratio between the motion of the hand and the collective pitch of the rotor is

$$\theta = \frac{\Delta\theta}{\ell_\phi \Delta\phi} \cdot z_{\text{hand}} = \frac{G_c}{\ell_\phi \Delta\phi} \cdot z_{\text{hand}}. \tag{7}$$

The parameters ℓ_ϕ and $\Delta\phi$ depend on the cockpit layout; the parameter G_c may depend on the rotor design; in augmented control designs it may even vary in flight, e.g. according to some scheduling. As a consequence, the sensitivity of the system behavior on these parameters is essential.

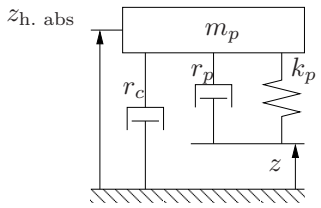

Figure 4: Structural model equivalent to Mayo's functions that describe the involuntary action of the pilot [21].

2.5. Pilot Model

A model of the 'active' behavior of the pilot was initially considered to assess its relevance for the analysis. The 'crossover' model proposed by McRuer [20] was used to formulate the behavior of a human operator that produces the plant control signal $\theta_{\text{AP}}(\text{j}\omega) = H_{\text{AP}}(\text{j}\omega)\varepsilon_y(\text{j}\omega)$ as a function of an error measure $\varepsilon_y(\text{j}\omega)$. Such model postulates that when it is put in feedback on a broad variety of tasks $y = H_{\text{task}}(\text{j}\omega)\theta(\text{j}\omega)$, it yields a Loop Transfer Function (LTF) which, in the vicinity of the crossover frequency ω_c, behaves as an integrator and an equivalent time delay τ_e,

$$H_{\text{task}}(\text{j}\omega)H_{\text{AP}}(\text{j}\omega) = \frac{\omega_c}{\text{j}\omega}\text{e}^{-\text{j}\omega\tau_e}. \tag{8}$$

When a position task is considered, i.e. $y \equiv z$, and thus $\varepsilon_y = z_{\text{desired}} - z$, a model of the vehicle further simplified with respect to that of Eqs. (2), obtained by considering only Eq. (2a) with $\beta \equiv 0$ and thus consisting of the dominant pole of the helicopter in addition to the integrator $1/s$, can be used to approximate H_{task},

$$H_{\text{task}}(s) \cong \frac{n_b\dfrac{\gamma}{6}\Omega^2\dfrac{I_\beta}{R}}{s\left(s\cdot m + n_b\dfrac{\gamma}{4}\Omega\dfrac{I_\beta}{R^2}\right)} = \frac{K_c}{s\,(Ts+1)}, \tag{9}$$

with $K_c = \Omega R$ and

$$T = \frac{m}{n_b\dfrac{\gamma}{4}\Omega\dfrac{I_\beta}{R^2}}, \tag{10}$$

the heave time constant. Eventually, after preliminary numerical results worked out any relevance for the collective bounce phenomenon, the AP was neglected.

A model of the 'passive' behavior of the pilot describes the involuntary control applied by the pilot as a consequence of the vibrations transmitted to the body by the cockpit. The biodynamics of the human body acts as a mechanical filter that modifies the amplitude and the phase of those vibrations while they are transmitted to the control inceptors via the pilot's limbs.

Table 2: Structural properties corresponding to Mayo's involuntary control models.

Mesomorphic pilot				
$k_p/m_p = \omega_p^2 =$	555.4	radian^2/s^2	$\omega_p = 3.75$	Hz
$(r_p + r_c)/m_p = 2\xi_p\omega_p =$	13.31	radian/s	$\xi_p = 0.28$	nondim.
$r_p/m_p =$	4.02	radian/s	$\tau_p = m_p/r_c = 0.10764$	s
Ectomorphic pilot				
$k_p/m_p = \omega_p^2 =$	452.3	radian^2/s^2	$\omega_p = 3.38$	Hz
$(r_p + r_c)/m_p = 2\xi_p\omega_p =$	13.7	radian/s	$\xi_p = 0.32$	nondim.
$r_p/m_p =$	5.19	radian/s	$\tau_p = m_p/r_c = 0.11751$	s

Consider the mechanical system of Fig. 4; the corresponding equation of motion, which describes the absolute vertical acceleration of the hand, $\ddot{z}_{\text{h. abs}}$, as a function of the vertical acceleration of the vehicle, $\ddot{z}$, in the Laplace domain, is

$$\ddot{z}_{\text{h. abs}} = \frac{s\dfrac{r_p}{m_p} + \dfrac{k_p}{m_p}}{s^2 + s\dfrac{r_p + r_c}{m_p} + \dfrac{k_p}{m_p}}\ddot{z}, \tag{11}$$

where $\ddot{z}$ is a shorthand for the vertical acceleration.

In [21], Mayo identified from experimental data a function with the structure of Eq. (11) to describe the involuntary action of helicopter pilots on the collective control inceptor when subjected to vertical vibration of the cockpit. The mass m_p, the stiffness k_p and the damping coefficient r_p represent the equivalent mechanical properties of a single degree of freedom model of the pilot's biomechanics; the coefficient r_c represents an additional damping directly associated with the rotation of the collective control inceptor. Lumped parameter models are relatively common in biodynamics, since the direct modeling of the dynamics of biological tissues is impractical for most applications [22]. Mayo identified the properties of two sets of pilots, called ectomorphic (small and lean build) and mesomorphic (large bone structure and muscle build). They are reported in Table 2. The poles associated with the pilot's biodynamics are well damped (about 30%). The frequency is about 3.5 Hz (compare it with the "three cycles per second" mentioned in the collective bounce accident reports), definitely below the coning frequency of light and medium helicopters, although relatively close and even above that of heavy ones.

As discussed in [23, 24, 25, 26], the output of Eq. (11) needs to be written as the relative acceleration of the hand with respect to the vehicle,

$$\ddot{z}_{\text{hand}} = \ddot{z}_{\text{h. abs}} - \ddot{z} = -s\frac{s + 1/\tau_p}{s^2 + 2\xi_p\omega_p s + \omega_p^2}\ddot{z}, \tag{12}$$

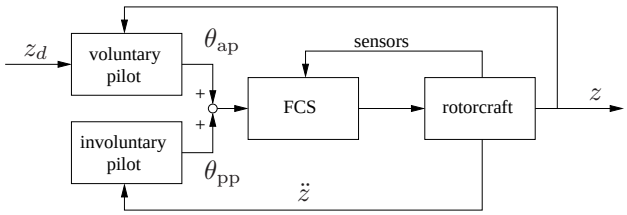

Figure 5: Block diagram of combined pilot voluntary (θ_{ap}) and involuntary (θ_{pp}) control interaction with the vehicle.

and integrated twice to yield the relative displacement of the hand, $z_{\mathrm{hand}} = \ddot{z}_{\mathrm{hand}}/s^2$. However, the double integration gives an integrator-like low-frequency asymptotic behavior, $1/s$, that is not physical (a pilot would always be able to compensate the error corresponding to a slow enough input) and overlaps with the AP behavior. The low-frequency asymptotic behavior can be corrected by adding a second-order high-pass filter with cutoff frequency ω_h slightly above the crossover frequency ω_c of the AP model. Since ω_c is less than 0.5 Hz, while the poles of the PP are at about 3.5 Hz, the bands of interest of the AP and PP models should be adequately separated. The combination of double integration and high-pass filtering yields

$$H_{\mathrm{PP}_f}(s) = -s\frac{s+1/\tau_p}{s^2+2\xi_p\omega_p s+\omega_p^2}\frac{1}{1+\sqrt{2}\dfrac{s}{\omega_h}+\left(\dfrac{s}{\omega_h}\right)^2}. \tag{13}$$

2.6. Loop Transfer Function

The loop is closed by feeding the combined AP and PP contributions to the collective pitch into the position task vehicle model, as shown in Fig. 5. The collective pitch

$$\theta = H_{\mathrm{AP}_f}(z_d - z) + \frac{G_c}{L_\psi \Delta\psi} H_{\mathrm{PP}_f} s^2 z, \tag{14}$$

fed it into the vehicle model, $z = H_{z\theta}\theta$, yields

$$\left(1 + H_{z\theta}\left(H_{\mathrm{AP}_f} - \frac{G_c}{L_\psi \Delta\psi} H_{\mathrm{PP}_f} s^2\right)\right) z = H_{z\theta} H_{\mathrm{AP}_f} z_d. \tag{15}$$

The LTF is thus the coefficient of z in Eq. (15) minus 1,

$$H_{\mathrm{L}} = H_{z\theta}\left(H_{\mathrm{AP}_f} - \frac{G_c}{L_\psi \Delta\psi} H_{\mathrm{PP}_f} s^2\right). \tag{16}$$

As anticipated, in the subsequent numerical analysis the transfer function that describes the intentional control exerted by the pilot, H_{AP_f}, is neglected.

It is worth mentioning that the Lynx has an autostabilizer on the collective, as reported by Padfield at page 159 of [16]; a control signal $\theta_{0a} = k_g \ddot{z}$, proportional to the normal acceleration, is fed back to the collective. Such contribution has not been considered because it is specific of that helicopter, and no data is available for the gain k_g.

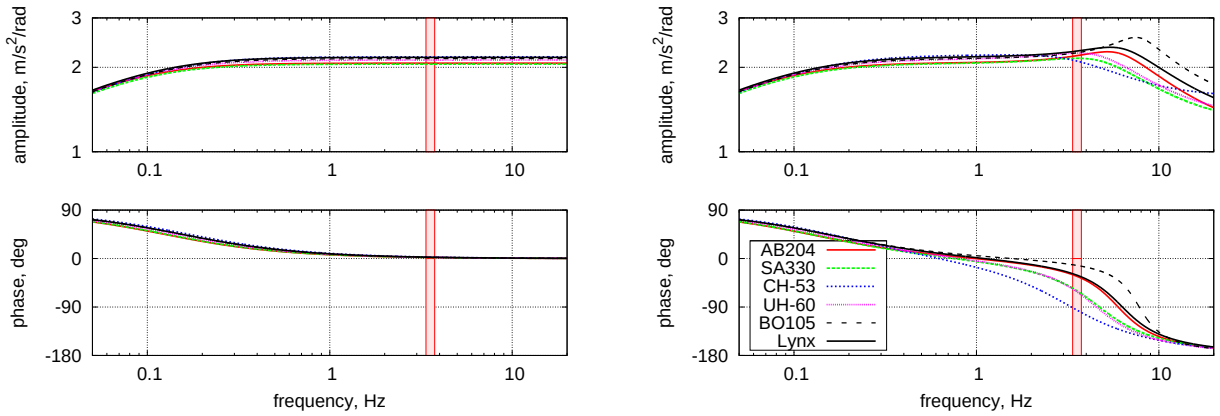

(a) Without coning mode.

(b) With coning mode.

Figure 6: Bode plot of vehicle acceleration as a function of collective pitch, $\ddot{z}(\mathrm{j}\omega)/\theta(\mathrm{j}\omega)$; the shaded (red) strip indicates the frequency band of relevance of the involuntary pilot dynamics.

3. Discussion of Results

The results in the present section highlight the proneness of helicopters to collective bounce according to a simplified model. The behavior of few helicopters with rather different properties and design is considered. Data come from rather heterogeneous sources, thus they may be not extremely accurate. For this reason, what emerges from the numerical results should not be seen as a direct comparison of the proneness to collective bounce of the helicopters considered in the analysis. On the contrary, the most important point is that fairly common trends appear; when differences surface, a clear explanation can be found in terms of a physical interpretation of the mathematics of the simplified model.

3.1. Acceleration Caused by Collective Input

The direct effect of a change in collective input is a nearly immediate change in thrust, which accelerates the helicopter. The transfer function between collective input and acceleration is shown in Fig. 6. The figure shows how the rotor coning mode affects the transfer function between the collective pitch and the vertical acceleration of the helicopter. The high-pass filter behavior induced by the pole at $\omega = n_b \gamma \Omega I_\beta/(4mR^2)$ is modified by a pair of complex conjugated poles at about the frequency of the blade coning mode. Since the coning mode is highly damped, the amplification is definitely limited, if any; however, in the vicinity of the coning mode frequency, and significantly right below it, a delay of up to 90 deg appears in the phase. It is this phase shift introduced by the coning mode that is essential for the emergence of the collective bounce instability, as will be shown in the closed loop analysis discussed in the following.

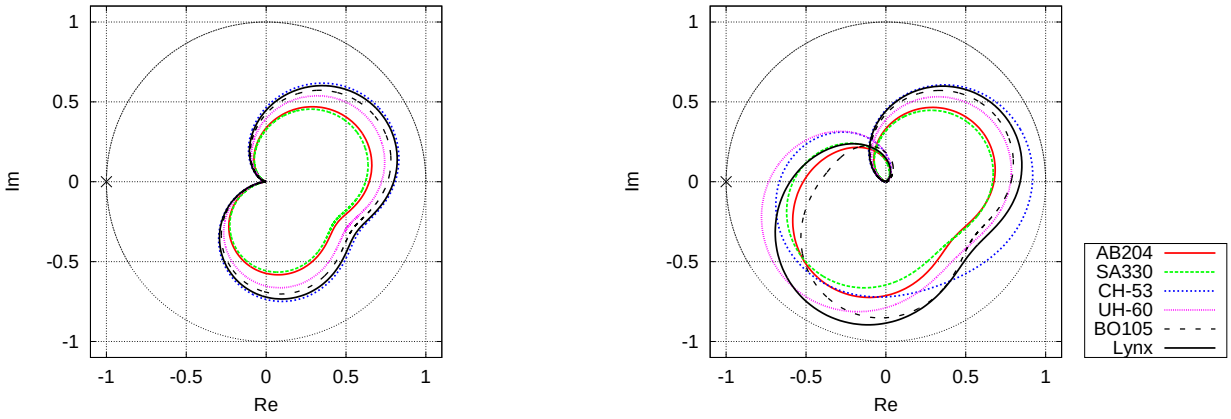

(a) Without coning mode.

(b) With coning mode.

Figure 7: Nyquist plot of LTF with pilot involuntary control model, nominal G_c.

3.2. Loop Closure on Vertical Displacement

When the loop is closed by the involuntary control of the pilot, the open loop behavior is modified as shown in the Nyquist plots of Fig. 7. The Nyquist plots of a stable system are very explicative because they intuitively express the degree of robustness of stability as the distance of each point of the LTF frequency response from the point $(-1+\mathrm{j}0)$ (see Chapter 7 of Ref. [27]). Often the robustness of stability is expressed using the concepts of gain and phase margin.[3] Figure 7(a) shows that when the coning mode is omitted, all the helicopters considered behave similarly, with exactly the same phase, and amplitudes that only differ by a minimal scale factor. Since the gain margin in this case is ∞, stability cannot be jeopardized by an increase of the gearing ratio G_c. Figure 7(b), on the contrary, shows that when the coning mode is considered, rather different behaviors appear in the vicinity of the poles associated with the involuntary behavior of the pilot. It is significant that, as already shown in Fig. 6(b), all helicopters with highly damped coning mode show a very small amplification factor compared with analogous results without coning mode, but with a phase lag that in the LTF is nearly 180 degrees in the band of relevance for the involuntary pilot dynamics, yielding a reduction of stability margins. The pilot's involuntary control dynamics produces a neat enlargement of the curves in the bottom left portion of the plot, which move towards point $(-1+\mathrm{j}0)$ and thus lose stability margins. So, *it is the phase shift rather than the amplification caused by the coning mode that increases the proneness of the helicopter to collective bounce.* This relatively obvious but essential observation has never been highlighted before, to the authors' knowledge. As one would expect, none of the helicopters analyzed shows unstable behavior; however, different proneness levels to PAO can be appreciated. It is remarkable, for

[3]The phase margin is the phase difference between the crossing of the LTF with the unit circle and -180 deg, namely $180+\angle(H_{\mathrm{L}}(\mathrm{j}\omega_{|H_{\mathrm{L}}|\equiv 1}))$. The gain margin is $1/|H_{\mathrm{L}}(j\omega_{(-180)})|$, the inverse of the magnitude of the LTF at ω corresponding to a -180 deg phase, i.e. $\mathrm{Re}(H_{\mathrm{L}}) \equiv -|H_{\mathrm{L}}|$; it must be larger than 1 for stability.

example, that helicopters with considerably large damping of the coning mode (SA330, CH-53 and UH-60, that is all the articulated rotor designs considered in this work) present the lowest gain margin. The Lynx, with hingeless main rotor design but relatively large damping of the coning mode, also shows a relatively low gain margin. On the contrary, the AB204 and the BO105, with relatively rigid rotors and low damping of the coning mode, show a larger gain margin. The latter design shows the largest gain margin, because the high rotor speed moves the coning mode away from the involuntary pilot's poles.

Since the pilot's involuntary dynamics poles are always at a frequency lower than the angular velocity of the main rotor, with the notable exception of the CH-53, low damping of the coning mode implies lower phase lag induced by this mode in the vicinity of the pilot poles, which dominate the amplitude of the LTF in the vicinity of 3.5 Hz.

3.3. Sensitivity to Take-Off Weight

Figure 8 shows the sensitivity of the LTF of the six helicopters to Take-Off Weight (TOW) ranging from 100% of the Maximum TOW (MTOW, inner curves) to 60% MTOW (outer curves).

Reducing the TOW reduces the stability margin essentially because for given values of the stability and control derivatives associated with the rotor, the vertical acceleration of the vehicle, which is fed to the involuntary pilot model, is scaled by a factor inversely proportional to the helicopter mass. All helicopters considered show a common trend.

3.4. Sensitivity to Lock Number

Figures 9 and 10 show the LTF for different values of Lock number. In Fig. 9, the Lock number is modified for constant blade inertia properties, thus virtually changing only the aerodynamic properties, i.e. the blade chord and thus the solidity $n_b c/(\pi R)$ of the rotor. The figure clearly shows that an increased Lock number adversely affects the stability of the LTF resulting from involuntary pilot control closure on the collective pitch. In all cases, an increase in Lock number (which is directly proportional to damping of the coning mode, according to Eq. (4)), causes an enlargement of the LTF curve. With the notable exception of the CH-53, for which the -180 degree phase occurs above the angular velocity of the rotor, the gain margin is reduced, in some cases significantly. The sensitivity of the LTF of the CH-53 is negligible in the portion of curve that is critical for stability. The largest sensitivity is shown by the BO105, the Lynx and, to some extent, the AB204. The squares in Fig. 9, associated with the frequency of the involuntary pilot control poles, also convey that the involuntary pilot control governs the proneness to instability, rather than the coning mode itself.

It is worth pointing out that since the Lock number is proportional to the air density ρ, it changes with the operating conditions. For example, when operating at ISA -40°C, the air density increases of about 15%; when operating at 15000 ft the air density decreases of about 35%. As a consequence, a variability

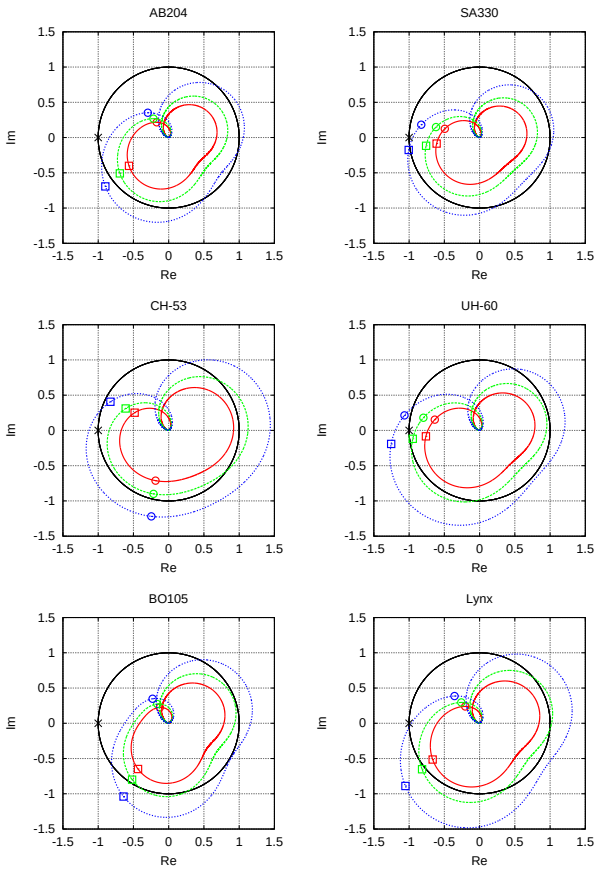

Figure 8: Nyquist plot of LTF with pilot involuntary control model for decreasing values of take-off weight from 100% MTOW (inner curves) to 60% MTOW (outer curves). Squares indicate the involuntary pilot frequency; circles indicate coning frequency.

even higher than that shown in Fig. 9 can be observed. A reduction in Lock number increases the stability margins, whereas an increase reduces them.

In the case of Fig. 10, the Lock number is modified by changing the inertia properties of the blade, for constant rotor solidity. The "rigid" (teeter, hingeless) helicopters are relatively insensitive to this parameter perturbation, whereas the articulated ones show slightly increased stability when the Lock number is increased, as opposed to the previous case. The difference between the two cases is that, despite analogous blade flapping dynamics, the change in Lock number resulting from a chord change directly modifies the control derivatives $T_{b/\theta} = \gamma\Omega^2 I_\beta/(6R)$ and $M_{\beta/\theta} = \gamma\Omega^2 I_\beta/8$ (the blade vertical force and moment about the flap hinge, namely the gradients of the left-hand sides of Eqs. (2) with respect to θ), while that resulting from a change in blade inertia properties leaves $T_{b/\theta}$ and $M_{\beta/\theta}$ unaffected. As a consequence, the former case

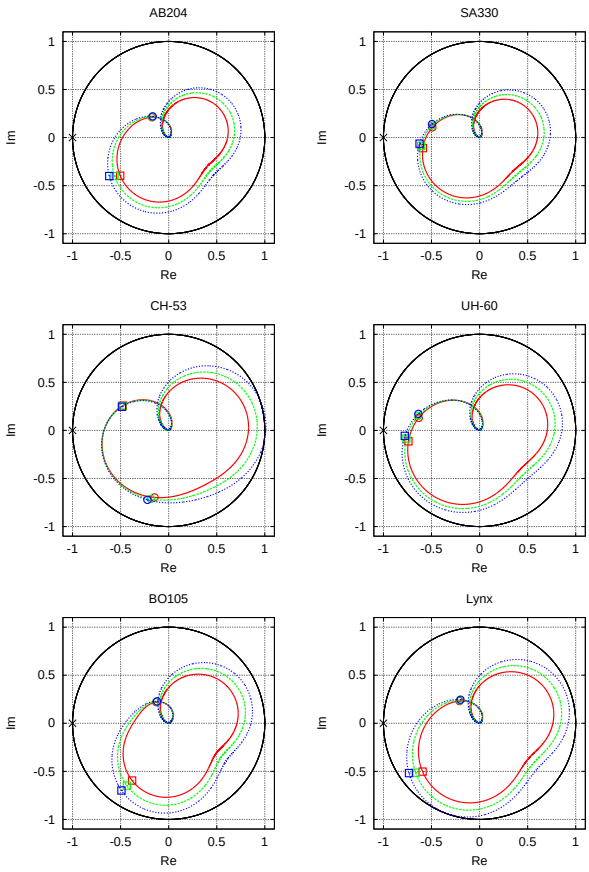

Figure 9: Nyquist plot of LTF with pilot involuntary control model for increasing values of Lock number γ at constant blade inertia properties from $\gamma_{\text{nom}} - 10\%$ (inner curves) to $\gamma_{\text{nom}} + 10\%$ (outer curves). Squares indicate the involuntary pilot frequency; circles indicate coning frequency.

resembles a change in gearing ratio G_c, i.e. an increase in Lock number also increases the gain of the LTF, and affects all helicopters especially at low frequency. Those with "stiff" hingeless rotor (AB204, BO105, Lynx) are mostly affected in the band of the coning mode. In the same band, the vehicles with articulated main rotor are mostly affected in the latter case, which otherwise does not produce significant changes.

3.5. Sensitivity to Fly-By-Wire Time Delay

As discussed in [28] (and in [29] with respect to the ADOCS fly-by-wire UH-60), excluding the time delay associated with the basic helicopter aeromechanics and the dynamics of the pitch control actuators, quantifiable in 50 to 100 ms and usually included in aeromechanics analysis, time delays are reported in the literature, ranging from 40 ms for DLR's ATTHeS (a modified BO105) to more than 100 ms for the ADOCS (a modified UH-60), the ARTI (a modified AH-64), and the NASA CH-47 test vehicles. Such delays are

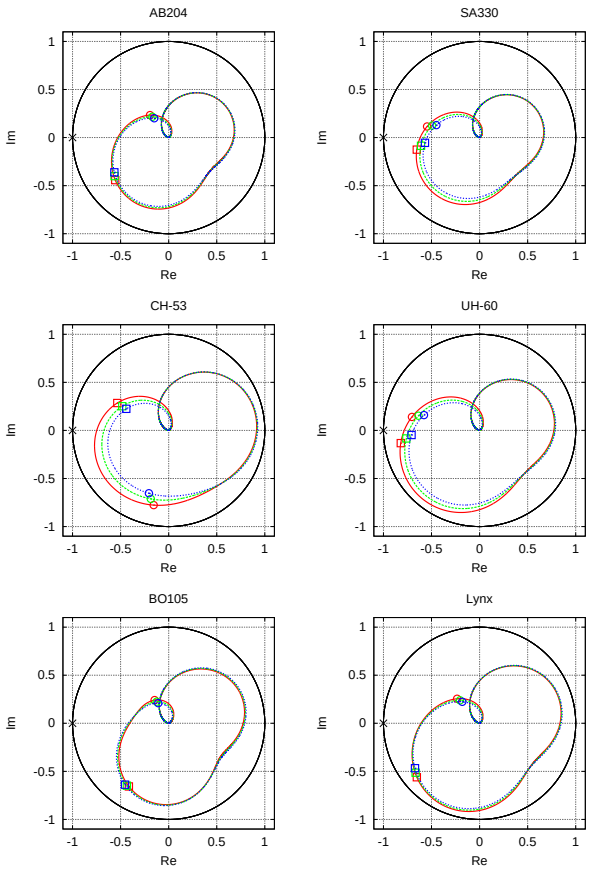

Figure 10: Nyquist plot of LTF with pilot involuntary control model for increasing values of Lock number γ at constant rotor solidity from $\gamma_{\text{nom}} - 10\%$ (outer curves) to $\gamma_{\text{nom}} + 10\%$ (inner curves). Squares indicate the involuntary pilot frequency; circles indicate coning frequency.

associated with stick filtering and control computer of Fly-By-Wire control systems.

Consider a time delay $\mathrm{e}^{-\tau s}$ between the pilot's involuntary input and the actual pitch command introduced in the simplified aircraft model. Its effect on the LTF corresponds to delaying the effect of the involuntary input. It causes a sort of 'clockwise rotation' of the curve that may reduce the gain margin, as shown in Fig. 11 for a time delay $\tau \cong 50$ ms.

3.6. Numerical Verification

To verify the analytical model presented in Section 2, detailed linearized aeroservoelastic models of the SA330 have been realized using data from [30, 16]. The models are assembled using the software MASST (Modern Aeroservoelastic State-Space Tools, [31, 32]). A detailed description of the models and their validation are presented in [33, 34, 35].

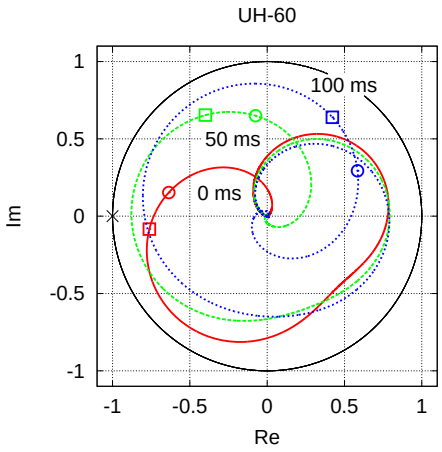

Figure 11: Nyquist plot of LTF with pilot involuntary control model, nominal G_c, with time delay τ ranging from 0 to 100 ms (data related to UH-60). Squares indicate the involuntary pilot frequency; circles indicate coning frequency.

Conventional helicopter models in MASST are composed by four sub-components: the airframe, the main rotor, the tail rotor and the servo-actuators. The airframe is characterized by 6 rigid body modes (Fore/Aft, Lateral, Plunge, Roll, Pitch and Yaw) with the appropriate aerodynamic stability derivatives, plus 8 elastic deformation modes in the range 5 Hz to 35 Hz, characteristic of airframe dynamics for this class of aircraft. The rotor dynamics are represented in the non-rotating reference frame using multiblade coordinates, resulting in a Linear Time Invariant (LTI) approximation for both hover and forward flight conditions, using the classic averaging approach in the latter case. Five modes per blade have been considered: the first lag mode, the first two flap bending modes, and the rigid pitch and first torsional modes. Details on connecting the rotor model to the airframe are given in [31, 32, 34, 35]. The aerodynamic model is based on blade element and momentum theory, using Pitt-Peters' dynamic inflow model [36]. The tail rotor is not modeled in detail; it is represented by a lateral force proportional to the tail rotor collective pitch control and to the lateral velocity at the rotor center, with stability derivatives from [16]. The servo-actuators are represented by transfer functions that model the dynamics of the servo-valve and the dynamic compliance [31, 35]. The complete LTI model of the SA330 consists of 73 states; the coefficients of each subcomponent are computed by linearization about appropriate trim conditions [31].

The LTI helicopter models show two low frequency unstable eigenvalues associated with the phugoid and Dutch roll flight mechanics modes. This is somewhat expected (see for example [16]). Since such dynamics are well separated in frequency from those of interest in the present work, the models have been decomposed into stable and unstable submodels, and only the stable submodel has been considered.

The stable model has been connected with the ectomorphic PP model of Eq. (13) excited by the vertical acceleration at the pilot's seat. The resulting contribution to the collective pitch has been input to the

swashplate actuators, yielding the LTF Nyquist plots of Figs. 12–15.

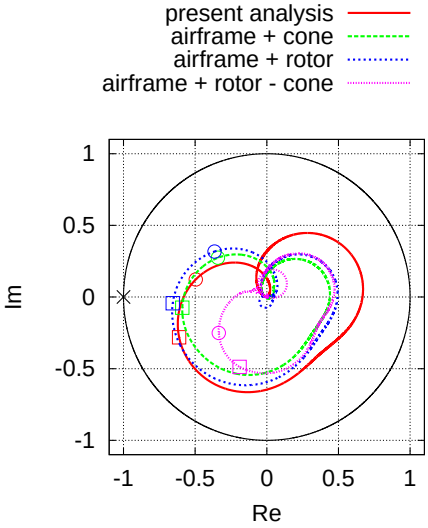

Figure 12: Nyquist plot of LTF with pilot involuntary control model, nominal G_c, for different numerical models of the SA330 helicopter in hover. Squares indicate the involuntary pilot frequency; circles indicate coning frequency.

Figure 12 compares the results in hover for models with different levels of detail. The Nyquist plot of the curve called 'airframe + cone' corresponds to a model with all the degrees of freedom of airframe and actuators, but only the rotor coning degree of freedom for the main rotor. The curve is very similar to those of Fig. 7, obtained with the simple analytical model presented in Section 2. By adding the remaining degrees of freedom of the main rotor (curve 'airframe + rotor'), the Nyquist plot changes minimally. On the contrary, if all main rotor degrees of freedom are considered along with the airframe modes, but the rotor coning mode is excluded (curve 'airframe + rotor − cone'), the Nyquist plot moves far away from the critical point $(-1 + \mathrm{j}0)$; its shape resembles the curve obtained using the analytical model without coning mode shown in Fig. 7(a), confirming the key role of the coning mode in collective bounce.

The effect of dynamic inflow on collective bounce is investigated in Fig. 13 by comparing the Nyquist plot of the SA330 model in hover with and without the inflow degree of freedom. The inclusion of axial dynamic inflow minimally reduces the amplitude margins for the points in the range of frequencies close to the critical point. The effect of the inflow on the Nyquist plot is significant at much lower frequencies; as a consequence, a stronger influence cannot be excluded on different rotorcraft. By comparing the low-frequency (rightmost) portion of the plots of Fig. 13 with those of Fig. 12, one can clearly appreciate how the curve 'present analysis' of Fig. 12 resembles the 'without inflow' one of Fig. 13. This further highlights the effect of the dynamic inflow on the LTF of interest, which at least in the case at hand is negligible in terms of impact on stability associated with involuntary pilot control.

The Nyquist plots obtained with and without the elastic degrees of freedom are compared in Fig. 14

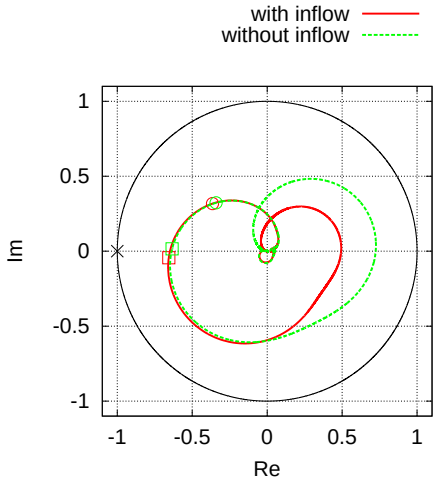

Figure 13: Nyquist plot of LTF with pilot involuntary control model, nominal G_c, for numerical models of the SA330 rotor in hover with and without inflow. Squares indicate the involuntary pilot frequency; circles indicate coning frequency.

to ascertain their effect. The addition of the airframe elastic degrees of freedom does not alter the nature of the phenomenon, which is dominated by the interaction of the pilot with the coning mode, although a non-negligible detrimental effect on the stability margins (as pointed out also in [25]) is clearly present.

Figure 15 shows the effect of the flight condition. The basic phenomenon remains the same, whereas a slight reduction of the stability margins is observed when the forward flight speed increases from 0 kts (hover) to 100 kts (an advance ratio μ of about 0.24).

3.7. Sensitivity to Other Parameters

One may legitimately ask whether other parameters have an impact on the collective bounce phenomenon either directly, or indirectly by affecting the phase delay between the vertical acceleration and the involuntary control input. In recent works, the collective bounce problem has been analyzed using analyses of higher fidelity than the one presented here. The models included rotor aeroelasticity modeled using nonlinear beams in a general-purpose multibody dynamics environment, blade element/momentum theory and boundary element method with prescribed and free wake, control system actuators dynamics (see for example [25]). It has been pointed out that the simple blade element/momentum theory (the same model the present analysis is based on) is able to capture the essence of the phenomenon, since it yields results comparable with those of higher fidelity methods, including free wake. Blade torsion and control system compliance also plays a role, by producing a larger actual static pitch (and thus aerodynamic loads) change that can be interpreted as an increase in gearing ratio G_c. The dynamics of the actuator may introduce further phase delay in the response, depending on their bandwidth. Their effect, analogous to what discussed in Section 3.5 about FBW delay, is mostly influential when the cut frequency is in the vicinity of the pilot biodynamics/rotor

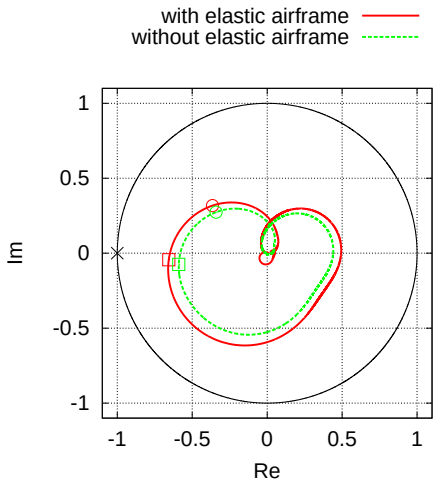

Figure 14: Nyquist plot of LTF with pilot involuntary control model, nominal G_c, for numerical models of the SA330 in hover with and without elastic airframe modes. Squares indicate the involuntary pilot frequency; circles indicate coning frequency.

coning frequency. The potential impact of drive train dynamics has not been investigated, essentially for the lack of sufficient information on the required properties. The opportunity to consider it, at least to assess whether it plays a role in the phenomenon, emerged since the activity in GARTEUR HC AG-16, but the lack of reliable data prevented its investigation. Frequency separation considerations (the dynamics of the fuel control system and the basic drive train dynamics should be well below the main rotor angular velocity) indicate that the participation should not be significant.

4. Possible Means of Prevention

The previous discussion highlighted how the collective bounce is rooted in the phase delay introduced by the main rotor coning motion. Prevention requires to either reduce involuntary collective control, or to reduce its effect on the vertical acceleration of the cockpit. Possible means are:

- open the feedback loop represented by the pilot's biomechanics, e.g. by introducing some nonlinearity that prevents or modifies the oscillation of the collective control; a typical solution consists in applying friction to the inceptor, which requires the pilot to overcome a threshold reaction moment to actually move the inceptor;
- modify the combined dynamics of pilot and collective inceptor; a typical solution consists in adding bobweights to increase the inertia of the inceptor and thus reduce the biomechanical frequency;
- eliminate the direct effect of the acceleration induced by a change in collective pitch and the motion of the inceptor by radically redesigning the collective control mechanism; for example, by replacing the

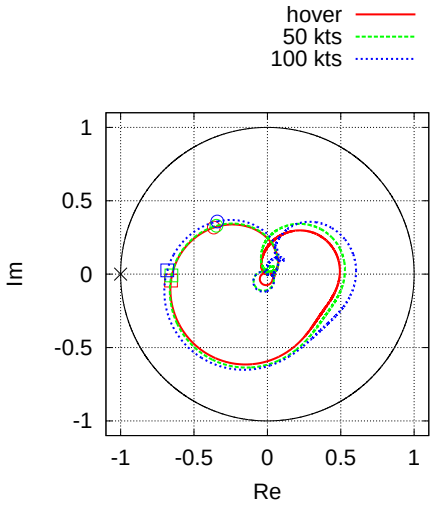

Figure 15: Nyquist plot of LTF with pilot involuntary control model, nominal G_c, for numerical models of the SA330 rotor in forward flight at different speeds. Squares indicate the involuntary pilot frequency; circles indicate coning frequency.

collective control inceptor with a thrust control lever similar to the throttle of fixed wing aircraft, or with a sidestick, a solution that may encounter reluctance in pilots;

- in fully or at least partially augmented rotorcraft, filter the unwanted dynamics at the FCS level.

Since the key factor of collective bounce appears to be the phase delay introduced by the rotor coning mode, the latter solution can be obtained by a filter between the collective requested by the pilot at the inceptor and the collective pitch commanded to the rotor blades. Such filter should introduce some lead (positive phase change) in the phase at the rotor coning frequency, to compensate for the lag naturally introduced by that mode, namely

$$H_{\mathrm{LL}}(s) = \frac{1 + s/z_{\mathrm{lead}}}{1 + s/p_{\mathrm{lead}}} \frac{1 + s/z_{\mathrm{lag}}}{1 + s/p_{\mathrm{lag}}}. \tag{17}$$

The desired effect is obtained with a low-frequency lag and a high frequency lead, i.e. $p_{\mathrm{lag}} < z_{\mathrm{lag}} \leq z_{\mathrm{lead}} < p_{\mathrm{lead}}$. Designing a filter for this purpose should be relatively simple, since the coning frequency is well known and only subjected to limited, predictable changes essentially related to the change of Lock number with air density. Since the frequency range of interest is very close to the SAS/FCS bandwidth, a thorough evaluation is needed to prevent side effects that may arise from the introduction of a device that affects the flight mechanics of the vehicle.

5. Conclusions

This work analyzes what is considered the root cause of helicopter collective bounce. It shows that the reduction of stability margins, and the possible development of instability, is rooted in the coupling

of the collective flap (or coning) mode of the rotor and the biodynamic mode of the pilot's arm holding the collective control inceptor, two highly damped modes when considered separately. The reduction of the stability margin is caused by the phase delay introduced by the coning mode, which reduces the phase in correspondence with the small amplification of the loop transfer function produced by the pilot's poles. A certain amount of feedback loop gain is needed to lead to instability. Since the phenomenon cannot be classified as a classical resonance between two structural modes (indeed, the phenomenon involves a structural mode, rotor coning, and the pilot's biodynamics; loss of stability is the consequence of a loss of phase margin, without significant amplitude amplification), it can hardly be addressed using notch filters, a classical means of prevention of structural coupling problems. Additionally, one of the elements of the feedback loop, the pilot's biodynamic response, shows significant uncertainty and variability, making the design of notch filters very challenging. A more robust solution could be the application of a lead-lag compensator that reduces the phase delay in the feedback loop in the vicinity of the coning frequency.

6. Acknowledgments

The research leading to these results has received funding from the European Community's Seventh Framework Programme (FP7/2007–2013) under grant agreement N. 266073.

[1] D. T. McRuer, Aviation Safety and Pilot Control: Understanding and Preventing Unfavourable Pilot-Vehicle Interactions, Washington DC: National Research Council, National Academy Press, 1997.

[2] D. G. Mitchell, D. H. Klyde, Identifying a PIO signature — new techniques applied to an old problem, in: AIAA Atmospheric Flight Mechanics Conference and Exhibit, Keystone, Colorado, USA, 2006, AIAA-2006-6495.

[3] O. Dieterich, J. Götz, B. DangVu, H. Haverdings, P. Masarati, M. D. Pavel, M. Jump, M. Gennaretti, Adverse rotorcraft-pilot coupling: Recent research activities in Europe, in: 34th European Rotorcraft Forum, Liverpool, UK, 2008.

[4] AGARD, PIO workshop following active control technology: Applications and lessons learned, CP 560, AGARD (1995).

[5] D. H. Klyde, D. G. Mitchell, A PIO case study — lessons learned through analysis, in: AIAA Atmospheric Flight Mechanics Conference, San Francisco, California, USA, 2005, AIAA-2005-5813.

[6] G. Weltz, K. Shweyk, D. Murray, Application of new and standard pilot-induced oscillation (pio) analysis methods to flight test data of the C-17 transport aircraft, in: AIAA Atmospheric Flight Mechanics Conference and Exhibit, Hilton Head, South Carolina, 2007, AIAA-2007-6387.

[7] J.-W. Perng, Application of parameter plane method to pilot-induced oscillations, Aerospace Science and Technology 23 (1) (2012) 140–145, doi:10.1016/j.ast.2011.06.006.

[8] J. Venrooij, D. Yilmaz, M. D. Pavel, G. Quaranta, M. Jump, M. Mulder, Measuring biodynamic feedthrough in helicopters, in: 37th European Rotorcraft Forum, Gallarate, Italy, 2011, pp. 199.1–12.

[9] M. D. Pavel, J. Malecki, B. DangVu, P. Masarati, M. Gennaretti, M. Jump, H. Smaili, A. Ionita, L. Zaicek, A retrospective survey of adverse rotorcraft pilot couplings in European perspective, in: American Helicopter Society 68th Annual Forum, Fort Worth, Texas, 2012.

[10] M. D. Pavel, M. Jump, B. Dang-Vu, P. Masarati, M. Gennaretti, A. Ionita, L. Zaichik, H. Smaili, G. Quaranta, D. Yilmaz, M. Jones, J. Serafini, J. Malecki, Adverse rotorcraft pilot couplings — past, present and future challenges, Progress in Aerospace Sciences 62 (2013) 1–51, doi:10.1016/j.paerosci.2013.04.003.

[11] M. D. Pavel, J. Malecki, B. DangVu, P. Masarati, G. Quaranta, M. Gennaretti, M. Jump, H. Smaili, A. Ionita, L. Zaicek, Aircraft and rotorcraft pilot coupling: a survey of recent research activities within the European project ARISTOTEL, in: 3rd CEAS Air & Space Conference, Venice, Italy, 2011.

[12] R. B. Walden, A retrospective survey of pilot-structural coupling instabilities in naval rotorcraft, in: American Helicopter Society 63rd Annual Forum, Virginia Beach, VA, 2007, pp. 1783–1800.

[13] R. W. Prouty, A. R. Yackle, The Lockheed AH-56 Cheyenne — Lessons learned, in: AIAA Aircraft Design Systems Meeting, Hilton Head, SC, USA, 1992, AIAA-1992-4278.

[14] T. Parham, Jr., D. Popelka, D. G. Miller, A. T. Froebel, V-22 pilot-in-the-loop aeroelastic stability analysis, in: American Helicopter Society 47th Annual Forum, Phoenix, Arizona (USA), 1991.

[15] G. Coppotelli, Experimental identification of the structural properties of an AB204 helicopter blade and finite element model validation, Experimental Techniques 33 (5) (2009) 25–34, doi:10.1111/j.1747-1567.2008.00447.x.

[16] G. D. Padfield, Helicopter Flight Dynamics: The Theory and Application of Flying Qualities and Simulation Modelling, Blackwell Publishing, 2007.

[17] W. R. Sturgeon, J. D. Phillips, A mathematical model of the CH-53 helicopter, TM 81238, NASA (1980).

[18] K. B. Hilbert, A mathematical model of the UH-60 helicopter, TM 85890, NASA (1984).

[19] R. Blackwell, T. Millott, Dynamics design characteristics of the Sikorsky X2 technology demonstrator aircraft, in: American Helicopter Society 64th Annual Forum, Montreal, Canada, 2008, pp. 1–13.

[20] D. T. McRuer, H. R. Jex, A review of quasi-linear pilot models, Human Factors in Electronics, IEEE Transactions on HFE-8 (3) (1967) 231–249, doi:10.1109/THFE.1967.234304.

[21] J. R. Mayo, The involuntary participation of a human pilot in a helicopter collective control loop, in: 15th European Rotorcraft Forum, Amsterdam, The Netherlands, 1989, pp. 81.1–12.

[22] M. J. Griffin, Handbook of Human Vibration, Academic Press, London, 1990.

[23] P. Masarati, G. Quaranta, M. Gennaretti, J. Serafini, An investigation of aeroelastic rotorcraft-pilot interaction, in: 37th European Rotorcraft Forum, Gallarate, Italy, 2011, Paper no. 112.

[24] P. Masarati, G. Quaranta, M. Jump, Experimental and numerical helicopter pilot characterization for aeroelastic rotorcraft-pilot couplings analysis, Proc. IMechE, Part G: J. Aerospace Engineering 227 (1) (2013) 124–140, doi:10.1177/0954410011427662.

[25] M. Gennaretti, J. Serafini, P. Masarati, G. Quaranta, Effects of biodynamic feedthrough in rotorcraft-pilot coupling: Collective bounce case, J. of Guidance, Control, and Dynamics 36 (6) (2013) 1709–1721, doi:10.2514/1.61355.

[26] G. Quaranta, P. Masarati, J. Venrooij, Impact of pilots' biodynamic feedthrough on rotorcraft by robust stability, Journal of Sound and Vibration 332 (20) (2013) 4948–4962, doi:10.1016/j.jsv.2013.04.020.

[27] S. Skogestad, I. Postlethwaite, Multivariable Feedback Control, John Wiley & Sons, Chichester, 2005.

[28] C. J. Ockier, Pilot induced oscillations in helicopters — three case studies, Tech. Rep. IB 111-96/12, German Aerospace Center (DLR), Braunschweig, Germany (1996).

[29] M. D. Takahashi, H_∞ helicopter flight control law design with and without rotor state feedback, J. of Guidance, Control, and Dynamics 17 (6) (1994) 1245–1251, doi:10.2514/3.21340.

[30] W. G. Bousman, C. Young, F. Toulmay, N. E. Gilbert, R. C. Strawn, J. V. Miller, T. H. Maier, M. Costes, P. Beaumier, A comparison of lifting-line and CFD methods with flight test data from a research Puma helicopter, TM 110421, NASA (October 1996).

[31] P. Masarati, V. Muscarello, G. Quaranta, Linearized aeroservoelastic analysis of rotary-wing aircraft, in: 36th European Rotorcraft Forum, Paris, France, 2010, pp. 099.1–10.

[32] P. Masarati, V. Muscarello, G. Quaranta, A. Locatelli, D. Mangone, L. Riviello, L. Viganò, An integrated environment for helicopter aeroservoelastic analysis: the ground resonance case, in: 37th European Rotorcraft Forum, Gallarate, Italy,

2011, pp. 177.1–12.

[33] V. Muscarello, P. Masarati, G. Quaranta, Multibody analysis of rotorcraft-pilot coupling, in: P. Eberhard, P. Ziegler (Eds.), 2nd Joint International Conference on Multibody System Dynamics, Stuttgart, Germany, 2012.

[34] V. Muscarello, P. Masarati, G. Quaranta, Robust aeroservoelastic analysis for the investigation of rotorcraft pilot couplings, Aerotecnica, Missili & Spazio 91 (1–2) (2012) 32–41.

[35] G. Quaranta, A. Tamer, V. Muscarello, P. Masarati, M. Gennaretti, J. Serafini, M. M. Colella, Rotorcraft aeroelastic stability using robust analysis, CEAS Aeronaut. J. 5 (1) (2014) 29–39, doi:10.1007/s13272-013-0082-z.

[36] D. M. Pitt, D. A. Peters, Theoretical prediction of dynamic-inflow derivatives, Vertica 5 (1) (1981) 21–34.